

Aggregation Kinetics of Alginate-Coated Hematite Nanoparticles in Monovalent and Divalent Electrolytes

KAI LOON CHEN,[†]
STEVEN E. MYLON,[‡] AND
MENACHEM ELIMELECH^{*†}

Department of Chemical Engineering, Environmental Engineering Program, Yale University, New Haven, Connecticut 06520-8286, and Department of Chemistry, Lafayette College, Easton, Pennsylvania 18042-1782

The early stage aggregation kinetics of bare and alginate-coated hematite nanoparticles are acquired through time-resolved dynamic light scattering (DLS). Varying concentrations of monovalent (NaCl) and divalent (MgCl₂ and CaCl₂) electrolytes are employed to induce aggregation. In the presence of NaCl and MgCl₂, the alginate-coated hematite nanoparticles undergo aggregation through electrostatic destabilization as described by the classic Derjaguin–Landau–Verwey–Overbeek (DLVO) theory. This is ascertained through examination of the favorable and unfavorable regimes of the stability curves depicting the attachment efficiency as a function of salt concentration. Additional evidence may be found in the aggregation kinetics of alginate-coated particles, which, under favorable aggregation conditions, are reasonably close to that of bare hematite nanoparticles. However, in the presence of CaCl₂, the aggregate growth rate of alginate-coated hematite nanoparticles is much higher than that which conventional diffusive aggregation predicts. Dispersed hematite primary particles and lower-order aggregates enmeshed within extended alginate gel networks were observed under transmission electron microscope (TEM). The proposed mechanism for enhanced aggregation suggests an apparent increase in the collision radii of alginate-coated hematite nanoparticles through alginate gel network formation from the particle surface. Additionally, cross-linking between unadsorbed (suspended) alginate macromolecules may form bridges between hematite-alginate gel clusters. It is further established that the presence of background electrolyte NaCl in solution is detrimental to the calcium-induced enhanced aggregation.

Introduction

The role of natural organic matter (NOM) in the fate and transport of inorganic colloidal particles in natural aquatic systems has been extensively studied (1–7). NOM is ubiquitous in natural waters and readily adsorbs to the surfaces of colloidal nanoparticles and suspended particulate matter. Adsorption of NOM modifies the surface characteristics of

the colloidal particles, thus playing a critical role in their stability and aggregation behavior.

NOM in natural aquatic systems mostly comprises humic substances and polysaccharides (8). Systematic studies demonstrated that adsorbed humic and fulvic acids can have a profound effect on the stability of colloidal particles (2, 4–7, 9). Studies have shown that humic substances stabilize colloidal particles via steric or electrostatic repulsion in the presence of monovalent salts, but this has not been the case for divalent cations such as Ca²⁺, Cu²⁺, and Pb²⁺, possibly due to cation complexation with the humic substances (2, 3, 6, 9). While a limited number of studies suggest that polysaccharides can destabilize colloidal particles (7, 10), their role in influencing the kinetics and mechanisms of colloid particle aggregation is still not well understood.

Polysaccharides make up 10–30% of the NOM in lakes (7, 10). In marine environments, the polysaccharide content may be as high as 50% of the dissolved organic carbon (DOC) (11, 12). Alginates are naturally occurring polysaccharides commonly found in marine environments (13, 14). They are produced by brown algae species, such as *Laminaria hyperborea*, *Ascophyllum nodosum*, and *Macrocystis pyrifera* (13). These alginates may be found as components of some algae cell walls, and are also likely to be excreted by the algae in the form of extracellular organic matter (15). Some bacteria, such as nitrogen-fixing *Azotobacter vinelandii* which can be found in soils (16, 17), and mucoid strains of *Pseudomonas aeruginosa*, also produce alginate as part of the extracellular polymeric substances (EPS) (13, 18–22). For these reasons, we used alginate as the model polyelectrolyte for polysaccharides in natural waters in this study.

Alginate is an unbranched block copolymer that comprises 1,4-linked β-D-mannuronic acid and α-L-guluronic acid residues. There are only three different block types that make up the polymer: mannuronic acid blocks, guluronic acid blocks, and the alternating mannuronic and guluronic acid blocks (13, 23). The proportions of the block types depend on the source of alginate (13). With the exception of Mg²⁺, divalent cations such as Ca²⁺, Sr²⁺, and Ba²⁺ can complex with the guluronic acid blocks of two neighboring alginate polymers. This form of binding is commonly referred to as the “egg-box structure”, whereby each divalent cation is coordinated with the guluronic acid residues (13, 14, 24). This results in the cross-linking of alginate polymers to form an extended gel network.

The objective of this study was to investigate the early stage aggregation kinetics of alginate-coated hematite nanoparticles in the presence of common monovalent (NaCl) and divalent (MgCl₂ and CaCl₂) electrolytes through time-resolved dynamic light scattering (DLS). The absolute aggregation rate constants of alginate-coated hematite nanoparticles were measured over a range of salt (NaCl, MgCl₂, and CaCl₂) concentrations and compared with those of bare hematite particles. The obtained aggregation kinetics results, along with the inspection of aggregate structure with a transmission electron microscope (TEM), were used to elucidate the aggregation mechanisms of hematite in the presence of polysaccharides. In particular, we highlight the critical role of alginate gel formation in controlling the aggregation behavior of hematite colloidal particles.

Materials and Methods

Alginate Source and Characterization. Commercially available sodium alginate (A2158, Sigma-Aldrich, St. Louis, MO) extracted from a brown algae species *Macrocystis pyrifera* was used in our study. According to the supplier, the alginate

* Corresponding author e-mail: menachem.elimelech@yale.edu; phone: (203) 432-2789.

[†] Yale University.

[‡] Lafayette College.

comprises approximately 61% mannuronic and 39% guluronic acid, and has a molecular weight ranging from 12 to 80 kDa. Size exclusion chromatography confirmed the molecular weight of the alginate to be between 20 and 80 kDa, with an average molecular weight of 49 kDa. The total organic carbon (TOC) content of the alginate was determined to be about 31% of its mass by high-temperature oxidation (TOC-V CSH/CSN, Shimadzu, Kyoto, Japan).

Potentiometric titration was conducted on sodium alginate using an auto-titrator (794 Basic Titrino, Metrohm, Herisau, Switzerland). A 100 mL solution of sodium alginate (100 mg/L) was purged with argon gas for at least 5 min to remove dissolved CO₂ before dilute HCl was added to lower the pH to 3. The alginate solution was then titrated with 0.1 M NaOH to pH 10. By comparing the amount of NaOH required to raise the pH of the alginate solution from 3 to 10 with that required to raise the pH of a blank solution, the carboxylic acidity of the alginate was determined to be 2.7 meq/g-alginate.

Hematite Nanoparticle Synthesis and Characterization.

Hematite nanoparticles were synthesized by forced hydrolysis of FeCl₃ (25), as described in our previous publication (2). The hematite stock concentration was found to be 5.5 g/L by gravimetric analysis. The hydrodynamic radius of the hematite nanoparticles was determined to be 37.4 nm (± 1.1 nm) through DLS (ALV-5000, Langen, Germany). TEM imaging of the hematite particles verified that the diameter of particles was about 75 nm, and that the particles were monodisperse and reasonably spherical with slight angular features. Assuming the nanoparticles to be perfectly spherical with diameter of 75 nm, and hematite specific gravity to be 5.3, we estimated the stock suspension to have a concentration of 4.5 × 10¹² particles/mL.

The alginate-coated hematite nanoparticles were prepared by adding 10 mL of the hematite stock solution to 35 mL of a solution of sodium alginate (700 mg/L) at pH 5.2. The resulting suspension was left aside for at least one month. The solution pH was maintained at 5.2 because this pH is favorable for alginate adsorption onto the hematite particles, which have an isoelectric point between pH 8 and 9 (26, 27). Note that the mannuronic and guluronic acids of alginate have pK_a values of about 3.2 and 3.6, respectively (28, 29). Stock solutions comprising hematite nanoparticles and alginate were centrifuged, and the TOC content of the supernatant was measured to determine the amount of alginate adsorbed onto the hematite. The unadsorbed alginate content of the stock solution was found to be 494 mg/L, and the degree of adsorption was 42.5 mg-alginate/g-hematite.

The electrophoretic mobilities of the bare and alginate-coated hematite nanoparticles were measured in the presence of 10 mM NaCl with the ZetaPALS analyzer (Brookhaven Instruments Corp., Holtsville, NY) at pH 12.2 and 5.2, respectively, at 25 °C. Electrophoretic mobilities were converted to ζ potentials by employing the tabulated values provided by Ottewill and Shaw (30), and the ζ potentials of the bare and coated hematite were determined to be -45 and -35 mV, respectively. The high ζ potentials ensured that the colloidal particles were stable prior to introduction of any destabilizing electrolyte.

Dynamic Light Scattering. The multi-detector light scattering unit (ALV-5000, Langen, Germany) was employed to conduct the DLS measurements. This unit utilized a solid-state diode-pumped, frequency-doubled Nd:vanadate (Nd:YVO₄) laser (Verdi V2, Coherent, Santa Clara, CA) that provided a single-frequency output with a wavelength of 532 nm. This unit also included 8 optical fiber photodetectors mounted on a compact goniometer system, and a thermostated index matching quartz vat filled with toluene doubly

filtered with 0.1 μm filters (Puradisc 25 TF, Whatman, Middlesex, UK). The room temperature was maintained at 23 °C.

New glass vials (Supelco, Bellefonte, PA) were soaked in cleaning solution (Extran MA01, Merck KGaA, Darmstadt, Germany) overnight, thoroughly rinsed with deionized water (Barnstead), and oven-dried under dust-free conditions before use. All vials were used only once. The bare and alginate-coated hematite stock suspensions were diluted between 3000 and 30 000 times with deionized water adjusted to the required pH with either HCl or NaOH. After dilution, the suspension concentration ranged from 7.5 × 10⁷ to 1.5 × 10⁹ particles per mL. In the case of the alginate-coated nanoparticles, the resulting unadsorbed alginate concentration in solution ranged from 37.4 to 74.8 μg/L after dilution. To induce aggregation, a predetermined amount of electrolyte stock solution, filtered with 0.1 μm filters (Anotop 25, Whatman, Middlesex, UK), was added to the vial holding 2 mL of diluted colloidal sample. The solution was vortexed briefly, inserted into the index matching vat, and DLS measurements were started immediately.

All light scattering measurements were conducted by employing the detector positioned at a scattering angle of 90° from the incident laser beam. The detector signal was fed into the correlator, which accumulated each autocorrelation function for 15 s. The intensity-weighted hydrodynamic radius of the colloidal aggregates was determined with second-order cumulant analysis (ALV software). The measurements were performed over time periods of between 20 min and 4 h because appropriate analysis of time-resolved DLS data requires approximately a 30% increase in the hydrodynamic radius. This provides adequate data to derive the aggregation kinetics of doublet formation, since the effective doublet hydrodynamic radius has been reported to be about 1.38 times the primary particle hydrodynamic radius (31).

Solution Chemistries. The aggregation experiments with the bare and alginate-coated hematite nanoparticles were conducted with monovalent (NaCl) and divalent (MgCl₂ and CaCl₂) electrolytes over a range of concentrations. The pH conditions of the bare and alginate-coated hematite nanoparticles were maintained at 12.2 ± 0.1 and 5.2 ± 0.1, respectively, under which the colloidal particles were stable at low ionic strengths.

Determination of Absolute Aggregation Rate Constant and Attachment Efficiency. Early stage aggregation kinetics can be described by the rate of doublet formation, which dominates over other higher-order aggregate formation. The loss in primary particles during the early stage of aggregation can be expressed as a second-order rate equation (32)

$$\left(\frac{dN_1}{dt}\right)_{t \rightarrow 0} = -k_{11}N_0^2 \quad (1)$$

where $N_1(t)$ is the concentration of primary particles as a function of time t , k_{11} is the absolute aggregation rate constant, and N_0 is the initial primary particle concentration, that is, $N_1(0) = N_0$. Since the loss of primary particles is primarily due to doublet formation at the initial aggregation stage, the rate of doublet formation can be expressed as

$$\left(\frac{dN_2}{dt}\right)_{t \rightarrow 0} = \frac{1}{2}k_{11}N_0^2 \quad (2)$$

where $N_2(t)$ is the concentration of doublets as a function of t .

Within the Rayleigh–Gans–Debye (RGD) approximation, which is valid for primary particles that are relatively small compared to the incident wavelength (31, 33), the absolute aggregation rate constant, k_{11} , can be determined through

time-resolved DLS measurements conducted at a fixed scattering angle based on the relationship (31, 34)

$$\frac{1}{r_h(0,q)} \left(\frac{dr_h(t,q)}{dt} \right)_{t \rightarrow 0} = k_{11} N_0 \left[1 + \frac{\sin(2aq)}{2aq} \right] \left(1 - \frac{1}{\delta} \right) \quad (3)$$

Here, q is the scattering vector defined by $(4\pi n/\lambda)\sin(\theta/2)$, with n being the refractive index of the medium, λ the wavelength of light, and θ the scattering angle; $r_h(t, q)$ is the hydrodynamic radius as a function of t and q ; a is the primary particle radius; and δ is the relative hydrodynamic radius of the doublet, which is approximately 1.38 (31). Since all DLS measurements were carried out at a fixed angle, the only independent variable in eq 3 is t , with r_h as the dependent variable.

To obtain k_{11} through eq 3, a linear least squares regression analysis of the increase in r_h with t was made. The boundary conditions for analysis required $r_h(0)$ to be within no more than 3 nm in excess of a and final r_h to be equal to approximately $1.3a$, where there are sufficient doublets formed and few higher-order aggregates. By constraining our analysis to these conditions, we were able to ensure consistency in our approach. The slope of the best fit line gives $(dr_h/dt)_{t \rightarrow 0}$, which is used in eq 3 to obtain k_{11} .

The attachment efficiency, α , otherwise known as the inverse stability ratio, $1/W$, is used to quantify the aggregation kinetics of colloidal systems. Attachment efficiencies are calculated by normalizing the measured k_{11} by the diffusion-limited aggregation rate constant $(k_{11})_{fast}$ determined under favorable aggregation conditions (2)

$$\alpha = \frac{k_{11}}{(k_{11})_{fast}} \quad (4)$$

The attachment efficiency α , ranging from 0 to 1, is the probability of an irreversible attachment resulting from the collision of two colloidal particles.

Observation of Aggregate Structures. Bare and alginate-coated hematite aggregates were observed through TEM. A Formvar- and carbon-coated nickel grid (100 mesh) was placed on a drop of aggregate sample (about 25 μ L) on a clean piece of laboratory film (Parafilm M, Pechiney Plastic Packaging, Menasha, WI) for about 2 min. Aggregation of the hematite nanoparticles was induced at particle concentrations 10–20 times higher than those employed in DLS experiments to allow for adsorption of a sufficient number of aggregates onto the grid. The grid was air-dried and examined under a Tecnai 12 Biotwin electron microscope (FEI) at 100 kV. Aggregate images were then captured on film or digitally recorded.

Results and Discussion

Aggregation of Bare Hematite in the Presence of Sodium Ions. We examined aggregation over a range of NaCl concentrations (6.4–283.0 mM) at pH 12.2 where the bare hematite nanoparticles are negatively charged and stable at low salt concentrations. Particle concentrations were determined depending on the electrolyte concentrations employed to achieve adequate aggregate growth over a reasonable time period. Figure 1a presents representative aggregation profiles of bare hematite nanoparticles at a concentration of 1.5×10^8 particles per mL for 4 different NaCl concentrations. DLVO-type interactions clearly dominate the aggregation behavior. At these low electrolyte concentrations (11.9 and 15.9 mM), any increase in the electrolyte concentration leads to a corresponding increase in the aggregation rate. However, at higher electrolyte

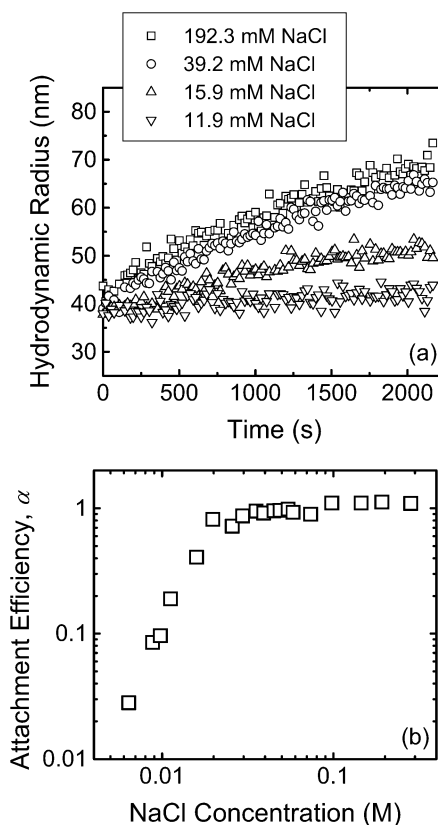


FIGURE 1. Aggregation of bare hematite nanoparticles in the presence of NaCl at pH 12.2. (a) Aggregation profiles at various NaCl concentrations at particle concentration of 1.5×10^8 particles per mL. (b) Attachment efficiencies as a function of NaCl concentration obtained over particle concentrations of 1.5×10^8 to 1.5×10^9 particles per mL. The CCC based on Figure 1b is 20 mM NaCl.

concentrations (39.2 and 192.3 mM), an increase in the electrolyte concentration has no influence on the aggregation rate.

To cover the broadest range of aggregation kinetics, DLS measurements were conducted with particle concentrations ranging from 1.5×10^8 to 1.5×10^9 particles per mL. Figure 1b presents the attachment efficiency α as a function of NaCl concentration. The attachment efficiency is dependent on NaCl concentration in the reaction-limited (unfavorable) regime ($\alpha < 1$), whereby an increase in the electrolyte concentration reduces the electrostatic energy barrier to aggregation between the negatively charged particles. However, in the diffusion-limited (favorable) regime ($\alpha = 1$), the electrolyte concentration is high enough to eliminate the energy barrier completely, resulting in diffusion-controlled aggregation. The critical coagulation concentration, CCC, where the energy barrier is just eliminated, demarcates the two regimes. For our bare hematite particles at pH 12.2, the CCC is about 20 mM NaCl, can be obtained from Figure 1b. Under favorable conditions, $(k_{11})_{fast}$ is determined to be 7.4×10^{-18} m³/s. A simple theoretical determination of the aggregation rate constant under diffusion-limited conditions yields $(k_{11})_{fast}$ of 1.22×10^{-17} m³/s at 23 °C (32). Our experimentally derived $(k_{11})_{fast}$ is smaller than the theoretical value, which is consistent with other studies employing various colloidal particles (31, 35).

Changes in Alginate Conformation with Ionic Strength.

The average hydrodynamic radius determined by DLS for stable alginate-coated hematite nanoparticles in both the absence and presence of NaCl and CaCl₂ electrolytes was measured prior to the aggregation studies. About 20 mea-

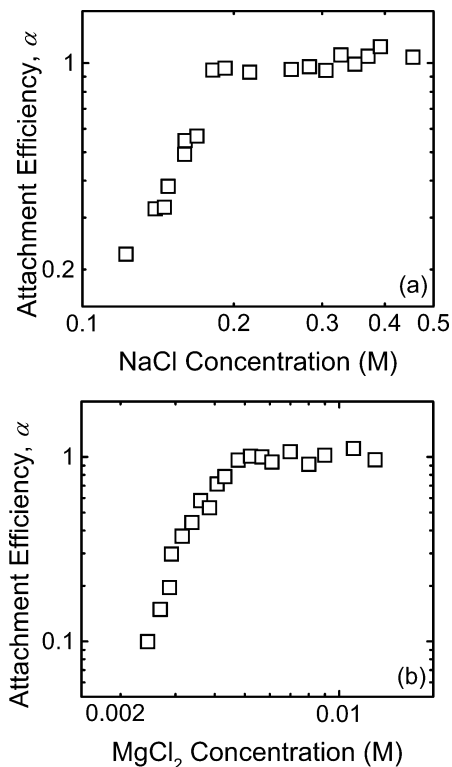


FIGURE 2. (a) Attachment efficiencies of alginate-coated hematite nanoparticles as a function of NaCl concentration at pH 5.2. The CCC based on these data is 180 mM NaCl. (b) Attachment efficiencies of alginate-coated hematite nanoparticles as a function of MgCl₂ concentration at pH 5.2. The CCC based on these data is 5 mM MgCl₂. For all aggregation experiments in a and b, the particle concentration employed is 1.5×10^8 particles per mL, and the unadsorbed alginate concentration in solution is 74.8 $\mu\text{g/L}$.

measurements of the hydrodynamic radius were made under each condition to determine the average hydrodynamic radius. With no added electrolytes, the average hydrodynamic radius of the alginate-coated hematite was 45.5 nm (± 1.3 nm). When the ionic strength was increased by introducing NaCl or CaCl₂ (19.8 and 1.0 mM, respectively), both at concentrations insufficient to induce aggregation, the average hydrodynamic radius of the alginate-coated particles decreased to 40.9 nm (± 0.7 nm) and 38.1 nm (± 1.0 nm), respectively. At these solution conditions, the alginate-coated particles were only slightly larger than the bare particles, which had an average hydrodynamic radius of 37.4 nm. This behavior is likely due to a change in the alginate polymer conformation on the hematite surface. Initially, the adsorbed alginate polyelectrolytes extend into bulk solution due to repulsive forces experienced between negatively charged functional groups along the polymers. The introduction of electrolytes results in electrostatic shielding (NaCl) and charge neutralization (CaCl₂) of alginate functional groups. Under these conditions, the polyelectrolytes can fold and retract toward the hematite surface, thus effectively reducing the hydrodynamic radius of the nanoparticles.

Aggregation of Alginate-Coated Hematite in the Presence of Sodium Ions. The attachment efficiency of the alginate-coated nanoparticles as a function of NaCl concentration (122.1–454.6 mM) at pH 5.2 is shown in Figure 2a. As described earlier, at this pH the alginate-coated nanoparticles possess a relatively high negative ζ potential and are quite stable at low and moderate NaCl concentration. The aggregation rate constants were measured at a single particle concentration of 1.5×10^8 particles per mL in order to maintain a constant unadsorbed alginate concentration

in solution of 74.8 $\mu\text{g/L}$. The distinct favorable and unfavorable regimes, demarcated by a CCC of about 180 mM NaCl, demonstrate electrostatic destabilization as the aggregation mechanism of the alginate-coated hematite nanoparticles in the presence of NaCl. Another piece of supporting evidence for this mechanism is that, under favorable conditions, $(k_{11})_{\text{fast}}$ is 6.9×10^{-18} m³/s, which is comparable to that of bare hematite (7.4×10^{-18} m³/s).

Aggregation of Alginate-Coated Hematite in the Presence of Magnesium Ions. The aggregation kinetics of alginate-coated nanoparticles were examined over a range of MgCl₂ concentrations (2.2–13.0 mM). Experimental conditions were similar to those in the presence of Na⁺. Figure 2b presents the attachment efficiency of the alginate-coated hematite as a function of MgCl₂ concentration, revealing aggregation behavior similar to that in NaCl. Electrostatic destabilization is the primary aggregation mechanism of the alginate-coated nanoparticles in MgCl₂, as verified by the two distinct regimes in the stability curve. The CCC observed was about 5 mM MgCl₂, and $(k_{11})_{\text{fast}}$ was determined to be 8.1×10^{-18} m³/s. The small difference in the fast absolute aggregation rate constants for Mg²⁺ and Na⁺ is acceptable, and has also been observed previously in other light scattering studies (31).

Enhanced Aggregation of Alginate-Coated Hematite in the Presence of Calcium Ions. The aggregation kinetics of alginate-coated nanoparticles have been studied at a CaCl₂ concentration of 9.0 mM. The aggregation behavior was compared with bare and alginate-coated hematite nanoparticles aggregated under the same experimental conditions in the presence of other electrolytes (NaCl and MgCl₂) under favorable conditions (Figure 3a). The aggregation profiles of the bare and alginate-coated nanoparticles in the presence of NaCl and MgCl₂ clearly overlap because aggregation occurs through electrostatic destabilization in the diffusion-limited regime. However, in the presence of CaCl₂, the aggregate growth rate of the alginate-coated nanoparticles was significantly higher. This enhanced aggregation behavior strongly suggests that the alginate-coated nanoparticles undergo a different aggregation mechanism in the presence of Ca²⁺ ions.

DLS measurements were also carried out with the alginate-coated nanoparticles over a range of CaCl₂ concentrations at pH 5.2. The particle concentration was decreased by 50% so that aggregate growth was slow enough to accurately capture the enhanced aggregation kinetics. This resulted in a concentration of 7.5×10^7 particles per mL and an unadsorbed alginate concentration in solution of 37.4 $\mu\text{g/L}$.

Because DLS results indicate that the alginate-coated nanoparticles do not undergo conventional aggregation through electrostatic destabilization in the presence of CaCl₂, an apparent aggregation rate constant, k_{app} , is used in place of k_{11} to quantify aggregation kinetics. The apparent rate constant replaces k_{11} in eq 3, and is derived in the same manner as discussed previously, with the other constants remaining unchanged. It is imperative to recognize that k_{app} no longer describes an absolute rate constant of *doublet formation* as does k_{11} . Instead, it serves to quantify the rate of *aggregate growth* in the early aggregation stage, without invoking any assumption regarding the aggregation mechanism. Likewise, an apparent attachment efficiency, α_{app} , is used to express the enhanced aggregation kinetics relative to diffusive aggregation kinetics, despite differences in their aggregation mechanisms:

$$\alpha_{\text{app}} = \frac{k_{\text{app}}}{(k_{11})_{\text{fast}}} \quad (5)$$

where $(k_{11})_{\text{fast}}$ of the alginate-coated nanoparticles (6.9×10^{-18} m³/s) was determined with NaCl under favorable conditions.

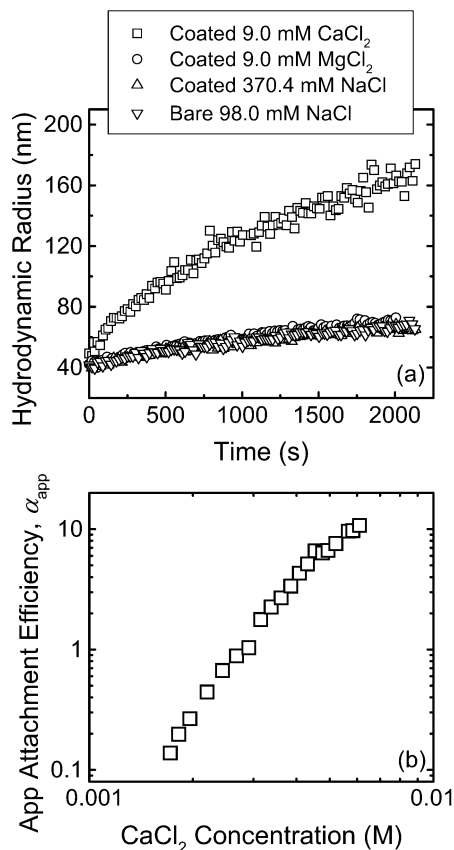


FIGURE 3. Enhanced aggregation of alginate-coated hematite nanoparticles in the presence of CaCl₂. (a) Comparison of aggregation profiles of bare and alginate-coated hematite nanoparticles in the presence of monovalent and divalent electrolytes. The bare hematite and alginate-coated hematite nanoparticles are aggregated at pH 12.2 and 5.2, respectively. For the four aggregation profiles, the particle concentration employed is 1.5×10^8 particles per mL, and the unadsorbed alginate content for the alginate-coated hematite samples is $74.8 \mu\text{g/L}$. (b) Apparent attachment efficiencies of alginate-coated hematite particles as a function of CaCl₂ concentration at pH 5.2. For all the aggregation experiments, the particle concentration employed is 7.5×10^7 particles per mL, and the unadsorbed alginate content is $37.4 \mu\text{g/L}$.

Equation 5 is similar to the common method of normalizing the initial slopes of aggregation profiles by the slope under favorable conditions, all derived at the same particle concentration (2, 6).

Figure 3b shows the apparent attachment efficiency of the alginate-coated nanoparticles as a function of CaCl₂ concentration, ranging from 1.7 to 6.1 mM. It was impossible to derive the aggregation kinetics at CaCl₂ concentration higher than 6.1 mM as the aggregate growth was too fast to capture sufficient hydrodynamic radius measurements before reaching 1.3a. Within the concentration range of CaCl₂ employed, no distinct favorable and unfavorable regimes were observed. The apparent attachment efficiency seems to increase linearly with CaCl₂ concentration. At concentrations above 2.9 mM, the experimental rate constant for aggregate growth was higher than what was previously observed under pure diffusion-limited aggregation, that is, $\alpha_{app} > 1$. At the highest CaCl₂ concentration (6.1 mM), our measured rate constants of aggregate growth were 10.7 times greater than those observed under pure diffusion-limited aggregation. This marked enhanced aggregation kinetics is very likely due to the ability of alginate to undergo gelation in the presence of Ca²⁺ cations, as will be discussed later in this paper. Table 1 summarizes the absolute aggregation rate constants under favorable aggregation conditions (k_{11})_{fast} for

TABLE 1. Summary of Absolute Aggregation Rate Constants, (k_{11})_{fast}, Obtained under Favorable (Non-Repulsive) Aggregation Conditions

electrolyte	bare hematite	alginate-coated hematite
NaCl	$7.4 \times 10^{-18} \text{ m}^3/\text{s}$	$6.9 \times 10^{-18} \text{ m}^3/\text{s}$
MgCl ₂	NM ^a	$8.1 \times 10^{-18} \text{ m}^3/\text{s}$
CaCl ₂	NM ^a	$7.4 \times 10^{-17} \text{ m}^3/\text{s}^b$

^a Not measured. ^b Apparent aggregation rate constant k_{app} obtained in the presence of the highest CaCl₂ concentration used (6.1 mM). k_{app} is used in place of k_{11} , because the aggregation mechanism of alginate-coated hematite in the presence of CaCl₂ is not the same as that of conventional diffusive aggregation.

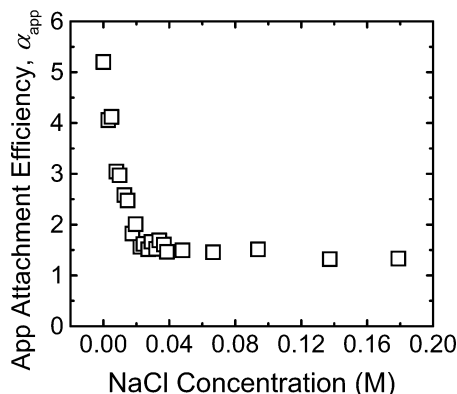


FIGURE 4. Apparent attachment efficiencies of alginate-coated hematite nanoparticles as a function of NaCl concentration at pH 5.2. CaCl₂ concentration is maintained at 4.7 mM for all the aggregation experiments. For all the aggregation experiments, the particle concentration employed is 7.5×10^7 particles per mL, and the unadsorbed alginate content is $37.4 \mu\text{g/L}$.

both the bare and alginate-coated nanoparticles in the presence of the different electrolytes used in this study.

Detrimental Effect of Background Sodium Ions on Enhanced Aggregation. We have also examined the aggregation kinetics of alginate-coated nanoparticles in the presence of both NaCl and CaCl₂ electrolytes. For these runs, CaCl₂ concentration was fixed at 4.7 mM for all the DLS measurements, while NaCl concentration was increased up to 179.0 mM. The experimental procedure was similar to previous DLS experiments, except that NaCl followed by CaCl₂ were introduced into the vial containing the particle suspension. Over the range of NaCl concentrations used, the rate of aggregation was extremely low. Hence, there was no concern that significant aggregation would have occurred within the time period between introductions of NaCl and CaCl₂.

The apparent attachment efficiency as a function of NaCl concentration is presented in Figure 4. At low NaCl concentrations, small increases in NaCl concentration resulted in substantial decreases in the apparent attachment efficiency. The apparent attachment efficiency tended toward 1 at NaCl concentrations higher than 80 mM, indicating diffusive aggregation to be the dominant aggregation mechanism. It is likely that Na⁺ ions compete with Ca²⁺ ions for the binding sites on the alginate polymers, thus reducing the extent of gel formation required for enhanced aggregation. This mechanism will be discussed in more detail in a later part of the paper.

Structure of Alginate-Coated Hematite Aggregates. TEM images revealed that aggregates of bare hematite nanoparticles formed under favorable conditions had open fractal structures that are consistent with previous studies (36, 37). Since the universal relationship of aggregate structures to the kinetics of colloid particle aggregation has been exten-

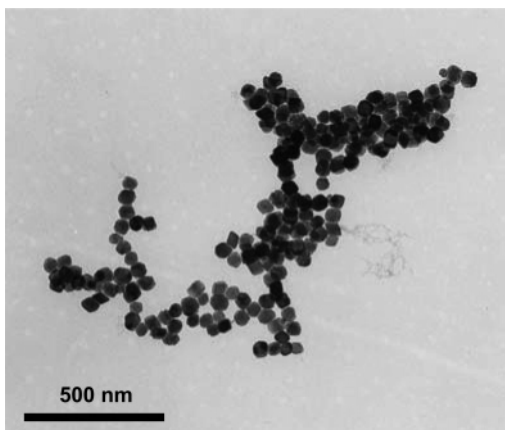


FIGURE 5. Alginate-coated hematite aggregate in the presence of 391.7 mM NaCl at pH 5.2. This corresponds to favorable aggregation conditions. Particle concentration is 1.5×10^9 particles per mL, and unadsorbed alginate content is 748 $\mu\text{g/L}$. Aggregation of the alginate-coated hematite particles is initiated about 3 to 4 h before the TEM images of the aggregates are captured. Aggregate structure is similar to ones found in the presence of 6.1 mM MgCl_2 at pH 5.2, which also corresponds to favorable aggregation conditions.

sively detailed and verified (38–41), it is not our intention to report the aggregate structure of bare nanoparticles. With the DLS experiments indicating differences in aggregation mechanisms of alginate-coated hematite nanoparticles in the presence of different cations (Na^+ and Mg^{2+} vs Ca^{2+}), greater interest lies in observing the aggregate structure of alginate-coated hematite with various cations. Studying the aggregate structure of alginate-coated hematite with various cations may provide more insights into the respective aggregation mechanisms.

For the TEM imaging studies, alginate-coated hematite nanoparticles were aggregated at a concentration of 1.5×10^9 particles per mL, with an unadsorbed alginate concentration of 748 $\mu\text{g/L}$ at pH 5.2 in NaCl, MgCl_2 , and CaCl_2 . The particle concentration employed was about an order of magnitude higher than that used in the DLS runs to generate more aggregates for sufficient adsorption onto the nickel grid. The aggregate structures were observed 3–4 h after aggregation was induced.

Figure 5 shows a representative aggregate structure of the alginate-coated hematite nanoparticles aggregated in 391.7 mM NaCl, which corresponds to favorable aggregation

conditions. The structures in 6.1 mM MgCl_2 , which also corresponded to favorable aggregation conditions, were similar to the ones in 391.7 mM NaCl. The aggregates had linear dimensions of about 1 μm , and open fractal structures which resulted from fast aggregation under favorable conditions. These results confirm that, with NaCl and MgCl_2 (not shown), the alginate-coated hematite had undergone aggregation through the same mechanism of electrostatic destabilization.

In 6.1 mM CaCl_2 , we observed hematite primary particles and lower-order aggregates held together within an extended network of an alginate gel. The combined hematite–alginate gel aggregates had linear dimensions 2–3 μm (Figure 6a and b). Focusing the electron beam on the aggregates under the microscope was done as quickly as possible before images were captured, because the electron beam used in the TEM may dehydrate or oxidize the alginate gel network. We noticed the gradual disappearance of a portion of the gel network if left focused under the electron beam for more than a few minutes.

The aggregate structures formed in the presence of Ca^{2+} in our study were interestingly similar to NOM–inorganic colloidal particle clusters found in lake waters (8). The strong similarity in both structures indicates that low concentrations of alginate/polysaccharide are sufficient for the enhanced aggregation to take place. In our systems, we were able to observe enhanced aggregation in solutions where the alginate concentration was as low as 37.4 $\mu\text{g/L}$. Due to the ubiquitous nature of alginate/polysaccharide in natural waters, it is likely that enhanced aggregation may be predominant in natural aquatic systems, especially when moderate concentrations of Ca^{2+} ions are present. Aggregates of the type we observed may be analogous to large polysaccharide heteroaggregates or the precursors to transparent exopolymer polysaccharides (TEP) in ocean waters (11, 12, 42).

Proposed Mechanism of Enhanced Aggregation with Calcium Ions. Enhanced aggregation is only observed in the presence of Ca^{2+} ions, but not with Na^+ and Mg^{2+} ions. From the TEM images, it was evident that the enhanced aggregation was due to the alginate gel network formation in the presence of Ca^{2+} ions.

Based on our results from the DLS experiments and TEM images, we propose the following enhanced aggregation mechanism. In the initial stage, the alginate-coated hematite nanoparticles and the suspended alginate content are stable in the absence of Ca^{2+} ions. Following the addition of CaCl_2 , some of the suspended alginate polymers undergo bridging

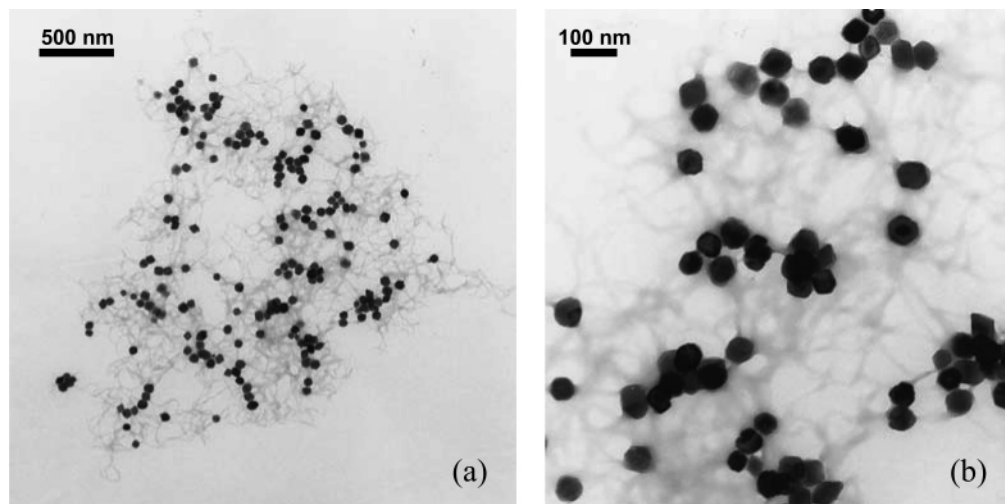
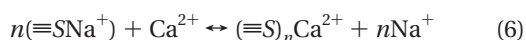


FIGURE 6. Combined hematite–alginate gel aggregate in the presence of 6.1 mM CaCl_2 at pH 5.2. a and b are TEM images of the same aggregate, but at different magnifications. Particle concentration is 1.5×10^9 particles per mL, and unadsorbed alginate content is 748 $\mu\text{g/L}$. Aggregation of the alginate-coated hematite nanoparticles is initiated about 3 to 4 h before the images of the aggregates are captured.

with the alginate on the hematite surface via calcium complexation. This effectively enlarges the collision radii of the suspended particles. Simultaneously, other suspended alginate polymers bind to each another via calcium complexation to form an alginate gel cluster. The alginate gel cluster acts as a bridge that binds the hematite clusters together. The combined effects of the larger collision radii of the alginate-coated nanoparticles and the alginate gel cluster formation significantly accelerate the rate of aggregate growth. The occurrence of direct attachment between the enlarged coated nanoparticles without the alginate gel bridging cannot be ruled out. The observation of lower-order hematite aggregates caught within the combined hematite–alginate gel aggregates (shown in Figure 6a and b) may be due to the simultaneous occurrence of aggregation of the nanoparticles while gel formation takes place in the early stage. This occurrence of lower-order aggregates has also been reported elsewhere (10) and observed within NOM–inorganic colloidal particle clusters in lake waters (8).

Although alginate has a higher affinity for Ca^{2+} than Na^+ cations due to the presence of guluronic acid blocks (14, 43), when the Na^+ concentration is large enough, the competition for binding sites between Na^+ and Ca^{2+} cations may have an effect on the alginate gel that is formed through calcium binding (13). Consequently, the influence of background electrolyte NaCl on the calcium-induced enhanced aggregation can be explained by the following ion-exchange relationship:



where $\equiv\text{S}$ represents a binding site on an alginate polymer, and n is the number of binding sites bound to a single Ca^{2+} cation. In the absence of Na^+ , all the binding sites are bound to Ca^{2+} ions, leading to the formation of egg-box structures binding the alginate polymers to form a gel network, thus resulting in enhanced aggregation. However, as the Na^+ concentration increases, Na^+ competes with Ca^{2+} ions for the binding sites along the alginate polymers, leading to less sites being available for calcium binding, which results in a smaller degree of enhanced aggregation. At high enough Na^+ concentration, the significant majority of sites are bound to Na^+ , and calcium binding of alginate polymers is no longer important. Instead, the presence of Na^+ and Ca^{2+} leads to shielding of the electrostatic repulsion experienced by the alginate-coated hematite nanoparticles. Thus, aggregation of the coated nanoparticles occurs through electrostatic destabilization, with diffusion controlling aggregation kinetics.

Acknowledgments

Funding was provided by the National Science Foundation (BES 0228911). We are grateful to Dr. Marc Pypaert (Department of Cell Biology, Yale University School of Medicine) for taking the TEM images used in this study. We also thank Professor Michal Borkovec and Dr. Paolo Galletto (of the Department of Inorganic, Analytical, and Applied Chemistry, University of Geneva) for providing K.L.C. training on the use of the light scattering setup.

Literature Cited

- Mosley, L. M.; Hunter, K. A.; Ducker, W. A. Forces between colloid particles in natural waters. *Environ. Sci. Technol.* **2003**, *37*, 3303–3308.
- Mylon, S. E.; Chen, K. L.; Elimelech, M. Influence of natural organic matter and ionic composition on the kinetics and structure of hematite colloid aggregation: Implications to iron depletion in estuaries. *Langmuir* **2004**, *20*, 9000–9006.
- Kretzschmar, R.; Sticher, H. Transport of humic-coated iron oxide colloids in a sandy soil: Influence of Ca^{2+} and trace metals. *Environ. Sci. Technol.* **1997**, *31*, 3497–3504.

- Tipping, E.; Higgins, D. C. The Effect of Adsorbed Humic Substances on the Colloid Stability of Hematite Particles. *Colloids Surf.* **1982**, *5*, 85–92.
- Amal, R.; Raper, J. A.; Waite, T. D. Effect of Fulvic-Acid Adsorption on the Aggregation Kinetics and Structure of Hematite Particles. *J. Colloid Interface Sci.* **1992**, *151*, 244–257.
- Heidmann, I.; Christl, I.; Kretzschmar, R. Aggregation kinetics of kaolinite–fulvic acid colloids as affected by the sorption of Cu and Pb. *Environ. Sci. Technol.* **2005**, *39*, 807–813.
- Wilkinson, K. J.; Joz-Roland, A.; Buffle, J. Different roles of pedogenic fulvic acids and aquagenic biopolymers on colloid aggregation and stability in freshwaters. *Limnol. Oceanogr.* **1997**, *42*, 1714–1724.
- Wilkinson, K. J.; Balnois, E.; Leppard, G. G.; Buffle, J. Characteristic features of the major components of freshwater colloidal organic matter revealed by transmission electron and atomic force microscopy. *Colloids Surf., A* **1999**, *155*, 287–310.
- Amirbahman, A.; Olson, T. M. Deposition Kinetics of Humic Matter-Coated Hematite in Porous-Media in the Presence of Ca^{2+} . *Colloids Surf., A* **1995**, *99*, 1–10.
- Buffle, J.; Wilkinson, K. J.; Stoll, S.; Filella, M.; Zhang, J. W. A generalized description of aquatic colloidal interactions: The three-colloidal component approach. *Environ. Sci. Technol.* **1998**, *32*, 2887–2899.
- Engel, A.; Thoms, S.; Riebesell, U.; Rochelle-Newall, E.; Zondervan, I. Polysaccharide aggregation as a potential sink of marine dissolved organic carbon. *Nature* **2004**, *428*, 929–932.
- Wells, M. L. Marine colloids – A neglected dimension. *Nature* **1998**, *391*, 530–531.
- Gombotz, W. R.; Wee, S. F. Protein release from alginate matrixes. *Adv. Drug Deliver. Rev.* **1998**, *31*, 267–285.
- Davis, T. A.; Llanes, F.; Volesky, B.; Mucci, A. Metal selectivity of *Sargassum* spp. and their alginates in relation to their α -L-guluronic acid content and conformation. *Environ. Sci. Technol.* **2003**, *37*, 261–267.
- Gregor, J. E.; Fenton, E.; Brokenshire, G.; Van Den Brink, P.; O'Sullivan, B. Interactions of calcium and aluminium ions with alginate. *Water Res.* **1996**, *30*, 1319–1324.
- Liermann, L. J.; Guynn, R. L.; Anbar, A.; Brantley, S. L. Production of a molybdophore during metal-targeted dissolution of silicates by soil bacteria. *Chem. Geol.* **2005**, *220*, 285–302.
- Gavini, N.; Hausman, B. S.; Pulakat, L.; Schreiner, R. P.; Williamson, J. A. Identification and Mutational Analysis of rfbG, the Gene Encoding CDP-D-Glucose-4,6-Dehydratase, Isolated from Free Living Soil Bacterium *Azotobacter vinelandii*. *Biochem. Biophys. Res. Commun.* **1997**, *240*, 153–161.
- Emmerichs, N.; Wingender, J.; Flemming, H. C.; Mayer, C. Interaction between alginates and manganese cations: identification of preferred cation binding sites. *Int. J. Biol. Macromol.* **2004**, *34*, 73–79.
- Lattner, D.; Flemming, H. C.; Mayer, C. ^{13}C NMR study of the interaction of bacterial alginate with bivalent cations. *Int. J. Biol. Macromol.* **2003**, *33*, 81–88.
- Cheze-Lange, H.; Beunard, D.; Dhulster, P.; Guillochon, D.; Caze, A. M.; Morcellet, M.; Saude, N.; Junter, G. A. Production of microbial alginate in a membrane bioreactor. *Enzyme Microb. Technol.* **2002**, *30*, 656–661.
- Chen, W. P.; Chen, J. Y.; Chang, S. C.; Su, C. L. Bacterial Alginate Produced by a Mutant of *Azotobacter-Vinelandii*. *Appl. Environ. Microb.* **1985**, *49*, 543–546.
- Saude, N.; Cheze-Lange, H.; Beunard, D.; Dhulster, P.; Guillochon, D.; Caze, A. M.; Morcellet, M.; Junter, G. A. Alginate production by *Azotobacter vinelandii* in a membrane bioreactor. *Process Biochem.* **2002**, *38*, 273–278.
- Bu, H. T.; Kjøniksen, A. L.; Knudsen, K. D.; Nyström, B. Rheological and structural properties of aqueous alginate during gelation via the Ugi multicomponent condensation reaction. *Biomacromolecules* **2004**, *5*, 1470–1479.
- Grant, G. T.; Morris, E. R.; Rees, D. A.; Smith, P. J. C.; Thom, D. Biological interactions between polysaccharides and divalent cations: The egg-box model. *FEBS Lett.* **1973**, *32*, 195–198.
- Matijević, E.; Scheiner, P. Ferric Hydrrous Oxide Sols. 3. Preparation of Uniform Particles by Hydrolysis of Fe(III)-Chloride, -Nitrate, and -Perchlorate Solutions. *J. Colloid Interface Sci.* **1978**, *63*, 509–524.
- Vermeer, A. W. P.; van Riemsdijk, W. H.; Koopal, L. K. Adsorption of humic acid to mineral particles. 1. Specific and electrostatic interactions. *Langmuir* **1998**, *14*, 2810–2819.
- Pochard, I.; Denoyel, R.; Couchot, P.; Foissy, A. Adsorption of barium and calcium chloride onto negatively charged α - Fe_2O_3 particles. *J. Colloid Interface Sci.* **2002**, *255*, 27–35.

- (28) Stefansson, M. Assessment of alginic acid molecular weight and chemical composition through capillary electrophoresis. *Anal. Chem.* **1999**, *71*, 2373–2378.
- (29) Baldursdottir, S. G.; Kjøniksen, A. L.; Karlsen, J.; Nyström, B.; Roots, J.; Tonnesen, H. H. Riboflavin-photosensitized changes in aqueous solutions of alginate. Rheological studies. *Bio-macromolecules* **2003**, *4*, 429–436.
- (30) Ottewill, R. H.; Shaw, J. N. Electrophoretic Studies on Polystyrene Latices. *J. Electroanal. Chem.* **1972**, *37*, 133–142.
- (31) Holthoff, H.; Egelhaaf, S. U.; Borkovec, M.; Schurtenberger, P.; Sticher, H. Coagulation rate measurements of colloidal particles by simultaneous static and dynamic light scattering. *Langmuir* **1996**, *12*, 5541–5549.
- (32) Elimelech, M.; Gregory, J.; Jia, X.; Williams, R. A. *Particle Deposition and Aggregation: Measurement, Modelling and Simulation*; Butterworth-Heinemann: Oxford, England, 1995.
- (33) Holthoff, H.; Borkovec, M.; Schurtenberger, P. Determination of light-scattering form factors of latex particle dimers with simultaneous static and dynamic light scattering in an aggregating suspension. *Phys. Rev. E* **1997**, *56*, 6945–6953.
- (34) Kleimann, J.; Gehin-Delval, C.; Auweter, H.; Borkovec, M. Superstoichiometric charge neutralization in particle–polyelectrolyte systems. *Langmuir* **2005**, *21*, 3688–3698.
- (35) van Zanten, J. H.; Elimelech, M. Determination of Absolute Coagulation Rate Constants by Multiangle Light-Scattering. *J. Colloid Interface Sci.* **1992**, *154*, 1–7.
- (36) Zhang, J. W.; Buffle, J. Multi-method determination of the fractal dimension of hematite aggregates. *Colloids Surf., A* **1996**, *107*, 175–187.
- (37) Amal, R.; Coury, J. R.; Raper, J. A.; Walsh, W. P.; Waite, T. D. Structure and Kinetics of Aggregating Colloidal Hematite. *Colloids Surf.* **1990**, *46*, 1–19.
- (38) Weitz, D. A.; Huang, J. S.; Lin, M. Y.; Sung, J. Limits of the Fractal Dimension for Irreversible Kinetic Aggregation of Gold Colloids. *Phys. Rev. Lett.* **1985**, *54*, 1416–1419.
- (39) Zhou, Z. K.; Chu, B. J. Light-Scattering Study on the Fractal Aggregates of Polystyrene Spheres – Kinetic and Structural Approaches. *J. Colloid Interface Sci.* **1991**, *143*, 356–365.
- (40) Kim, A. Y.; Berg, J. C. Fractal aggregation: Scaling of fractal dimension with stability ratio. *Langmuir* **2000**, *16*, 2101–2104.
- (41) Rarity, J. Flocculation – Colloids Stick to Fractal Rules. *Nature* **1989**, *339*, 340–341.
- (42) Chin, W. C.; Orellana, M. V.; Verdugo, P. Spontaneous assembly of marine dissolved organic matter into polymer gels. *Nature* **1998**, *391*, 568–572.
- (43) Smidsrød, O.; Haug, A. Effect of Divalent Metals on Properties of Alginate Solutions. I. Calcium Ions. *Acta Chem. Scand.* **1965**, *19*, 329–340.

Received for review September 12, 2005. Revised manuscript received December 18, 2005. Accepted January 5, 2006.

ES0518068